Computer Life
ISSN: 1819-4818 | Vol. 13, No. 1, 2025

Numerical Simulation and Analysis of the Vibration Characteristics of the String Vibration Screen Mesh

Zhiheng Wang*, Zhongbin Liu[a]

College of Mechanical Engineering, Sichaun University of Science & Engineering, Yibin, Sichuan, 643002, China
* **Corresponding author**: Zhiheng Wang (Email: 981092304@qq.com), [a] Lzbxxh@163.com

Abstract: With the deepening of oil and gas drilling, the increase of ultrafine particles and the complexity of waste water-based drilling mud have intensified the difficulty of solid-liquid separation. This paper addresses problems such as screen mud cake and clogging of fine mesh screens during the operation of drilling fluid vibrating screens. A novel string vibration-based detachment process is proposed, utilizing a single excitation source to induce string vibration in the filter screen. This promotes the detachment of filter cake from the separation membrane, reduces membrane fouling, and facilitates the regeneration of the filtration medium. The physical method improves the dehydration efficiency of waste mud and the recovery of the liquid phase. A string vibration model of the filter screen is established to study the amplitude, acceleration, and stress-strain characteristics under different vibration frequencies. Results show that the amplitude fluctuations of surface particles on the filter screen follow a parabolic trend with frequency variation; amplitude fluctuations near the edges of the screen are greater than at the center, with the most pronounced fluctuations occurring at 40 Hz. Particles near the excitation source exhibit strong periodic oscillations. Acceleration varies significantly with frequency, showing intense fluctuations between 40 Hz and 50 Hz. Surface particle oscillations are periodic, with rapid velocity fluctuations near the excitation source. When the frequency exceeds 40 Hz, acceleration sharply increases, then drastically decreases after 60 Hz. Compared with traditional vibrating screens, the string vibration process produces heterogeneous particle oscillations on the filter surface with higher acceleration magnitudes and faster variation rates, thereby facilitating more effective detachment of materials.

Keywords: String vibration; Resonance effect; Vibration characteristics; Filter detachment.

1. Introduction

Petroleum and natural gas constitute essential components of a nation's energy supply, directly influencing national development and the quality of life of its citizens. Crude oil has a broad spectrum of applications; in addition to serving as a primary fuel source, it is a key raw material in the production of asphalt, rubber, and various plastic products. Natural gas, widely recognized for its cleanliness and efficiency, plays an increasingly important role in both domestic and industrial energy consumption [1-2]. Drilling operations inevitably generate substantial amounts of solid waste. Among these, waste drilling mud is of particular concern due to its complex composition, which typically includes high concentrations of mineral oil and polymeric compounds. This waste mud often forms a water-in-oil emulsion system. Notably, each cubic meter of drilling mud may contain base oils and chemical additives valued at tens of thousands of yuan, underscoring the significant economic and environmental incentives for effective treatment and resource recovery [3-4], Maximizing the recovery of valuable liquid phases from waste drilling mud, followed by the environmentally responsible treatment or disposal of the remaining solid phases, has become a key research focus in the oil and gas industry.

As oil and gas drilling depths continue to increase, the proportion of ultra-fine particles in waste drilling mud rises, and the complexity of the mud system intensifies, making liquid–solid separation increasingly challenging. Currently, the industry commonly employs chemical destabilizing agents to break the colloidal structure for phase separation. However, drilling fluids treated through such methods are typically difficult to recycle and reuse, limiting their applicability in closed-loop systems [5]. Mechanical separation methods have been explored as an alternative approach to achieve phase separation without disrupting the stability of the drilling fluid system. However, these methods are often associated with low separation efficiency and require multiple processing steps, which limit their practicality and large-scale application. Currently, the treatment of waste water-based drilling fluids is generally categorized into primary dewatering and advanced (deep) dewatering. In primary dewatering, a combination of shale shaker screening and pressure filtration is typically employed, which can reduce the water content to below 60%. In the Bohai Oilfield [6], integrated skid-mounted units combining flocculation and pressure filtration have been employed, further reducing the moisture content of the filter cake to approximately 45%. For advanced dewatering [7], some commercially available cuttings dryers are capable of lowering the moisture content to around 10%–15%. After chemical pretreatment (e.g., with flocculants) followed by centrifugation [8], the moisture content of the filter cake is reduced to approximately 55%., which falls significantly short of industry standards.

Current research on mechanical separation continues to focus primarily on improving the performance of high-frequency vibrating screens. In 2014, Derrick Corporation [9] introduced the MONGOOSE PRO series of high-frequency vibrating screens, featuring a modular design and utilizing 180-mesh screens, with a processing capacity of up to 180 m^3/h. Song [10] et al. proposed a novel method to enhance vibration intensity by employing a multi-degree-of-freedom elastic screen surface, which replaces the traditional rigid screen while maintaining the original vibration parameters. This approach effectively mitigates screen clogging issues.

Yin P [11] et al. developed a vibration screening device based on periodic negative pressure, in which pulsed vacuum airflow combined with mechanical vibration governs the movement of material particles on the screen surface. The motion characteristics are primarily influenced by vibration frequency and amplitude, while the pulsed vacuum addresses screen adhesion and blockage, significantly enhancing solid–liquid separation efficiency. Similarly, Menezes A.L[12]. et al. designed a vibration–negative pressure gradient synergistic dewatering screen, where a vacuum pump creates negative pressure beneath the drying area of the screen, thereby increasing the pressure gradient along the material layer thickness and improving the dewatering performance.

During the dewatering of ultrafine slurry on vibrating screens, the process exhibits the characteristics of a multiphase fluid dynamic percolation system. From the feed inlet to the discharge outlet, several complex and interrelated phenomena occur, including gradual changes in the solid–liquid ratio, dynamic interactions between solid and liquid phases, liquid seepage through viscous material layers, particle-induced aperture clogging, and water film blockage of screen pores. Each stage of the dewatering process displays distinct behaviors that are mutually constrained, resulting in a highly complex flow regime. The slurry morphology on the screen surface demonstrates a nonlinear spatial distribution, indicating that uniform vibration parameters across the screen surface are incompatible with the evolving dynamics of vibratory dewatering. The conventional negative-pressure vibrating screen [13], in which the screen mesh vibrates together with the screen box, can no longer meet the dewatering requirements of current complex materials.

The In response to the common issues of screen blinding and clogging encountered with fine-mesh screens during the operation of drilling fluid shakers, this study proposes a novel string vibration–based desorption technique. The method employs a single excitation source to induce string-like vibrations in the screen mesh, thereby promoting the detachment of filter cakes from the separation membrane, reducing membrane fouling, and enhancing the regeneration of the filtration medium. This purely physical approach aims to improve both the dewatering efficiency of waste drilling mud and the recovery rate of the liquid phase. The focus of this work is to investigate the vibration characteristics of the screen mesh, with particular attention to its string vibration behavior. A vibration analysis model for the string-like deformation of the mesh is established, and flexible multibody dynamics is employed to simulate the vibration response of surface particles on the screen. Through simulation under various vibration frequencies, the study analyzes the mesh vibration characteristics and explores the mechanism by which string vibration enhances desorption and liquid–solid separation in the context of an elastic screen.

2. Mathematical Model of String Vibration

Assuming that the length of the string is much greater than the actual vibration amplitude, the string is distributed along the x-axis, with its equilibrium position located on the positive half of the x-axis, and the vibration occurring in the y-axis direction, as shown in Figure 1.

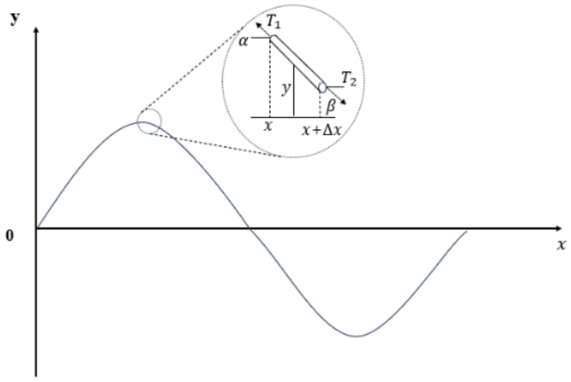

Fig.1 Schematic diagram of the theoretical model of string vibration

A small segment of the string is considered for elemental analysis, and the total length of the string is assumed to be L. The string segment per unit length is subjected to an external force $f(x,t)$, with an average linear density of ρ. A tensile force T is applied at both ends of the string. The angles between the string segment ends and the horizontal axis are α and β, respectively. An equivalent damping coefficient R is considered, and the displacement variation is denoted by $y(x,t)$. Consequently, the governing equation for the string vibration [14] is expressed as:

$$\frac{\partial^2 y}{\partial t^2}+R\frac{\partial y}{\partial t}-\frac{T}{\rho}\frac{\partial^2 y}{\partial x^2}=\frac{f(x,t)}{\rho} \tag{1}$$

The boundary and initial conditions at this time are:

$$\begin{cases} y(x,0)=0 \\ y(l,t)=y(0,t)=0 \end{cases} \tag{2}$$

Based on the above theoretical analysis of string vibration, the transverse forced vibration equation of the string can be derived as:

$$\frac{\delta^2 u}{\delta t^2}=a^2\frac{\delta^2 u}{\delta x^2}+f(x,t) \tag{3}$$

where $f(x,t)$ is the driving force, ρ is the mass per unit length of the screen mesh, and T is the tension of the screen mesh.

Free transverse vibration of the screen mesh:

$$\frac{\delta^2 u}{\delta t^2}-a^2\frac{\delta^2 u}{\delta x^2}=0 \tag{4}$$

At the initial stage of vibration, the screen mesh is influenced by its own weight, and its axis of symmetry coincides with the vertical line at $x=l/2$. The initial conditions are:

$$\begin{cases} u(x,0)=\dfrac{4hx(l-x)}{l} \\ \dfrac{\partial u(x,0)}{\partial t}=0 \end{cases} \tag{5}$$

By applying the method of separation of variables to the above equation, the solution is obtained as:

$$\mathrm{u}_1(\mathrm{x},\mathrm{t})=\frac{32h}{\pi^3}\sum\nolimits_{m=0}^{\infty}\frac{1}{(2m+1)^3} \cos\frac{(2m+1)\pi\alpha}{1}t\sin\frac{(2m+1)\pi}{1}x \tag{6}$$

Forced vibration of the string:

$$\frac{\partial^2 u_2}{\partial t^2} - \alpha \frac{\partial^2 u_2}{\partial x^2} = F(x,t) \tag{7}$$

Assuming that the initial displacement and initial velocity of the screen mesh are both zero, and that the vibrator follows a simple harmonic motion described by the equation $p_1(x,t) = A\sin\omega t$, where A is the vibration amplitude, the boundary conditions are therefore:

$$\begin{cases} u_2(0,t) = 0 \\ u_2(x,t) = A\sin\varphi t \end{cases} \tag{8}$$

The solution is obtained as:

$$u_2(x,t) = \sum_{n=1}^{\infty} \left(\frac{2Al^2\left[1-(-1)^n\right]}{n\pi\left[(n\pi\alpha)^2-(\omega l)^2\right]} \sin\alpha t - \frac{2A\alpha l^3\left[1-(-1)^n\right]}{\pi^2 n^2 \alpha\left[(n\pi\alpha)^2-(\omega l)^2\right]} \cos\frac{n\pi}{l}\alpha t \right) \sin\frac{n\pi x}{l} \tag{9}$$

The vibration induced by string oscillation is the superposition of the screen mesh's free vibration and the vibration response under external excitation [15]. The general solution to the overall string vibration equation is

$$u = u_1 + u_2$$

3. Numerical Analysis Model of String Vibration

3.1. Establishment of the Simulation Model

To reduce computational complexity, save time, and obtain simulation results efficiently, the simulation model is appropriately simplified during the modeling process. The simplified model is shown in Figure 2:

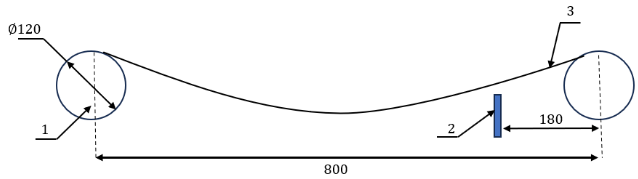

Fig.2 Structure size diagram

(1) Bolts and other small connecting components are removed and replaced with mass-equivalent simplifications.

(2) Supporting components such as the frame are removed, and the main components are fixed on a plane using constraint joints.

Table 1. Structural parameters of the separation belt

Name	Parameters
Material	304 stainless steel
Density（g/m^2）	7.93
Length（mm）	800
Width（mm）	400
Thickness（mm）	2
Young's Modulus（N/mm^2）	2000

In this study, the Fflex module in RecurDyn is employed to model the screen mesh as a flexible body. The excitation plate in the vibration system has structural parameters of 120 mm in length and 10 mm in width, and is made of acrylic. A translational joint is defined between the excitation plate and the ground to apply a prescribed simple harmonic motion. The parameters of the screen mesh are listed in Table 1.

3.2. Simulation Conditions and Settings

To facilitate observation of the overall oscillation behavior of the screen mesh during string vibration, marker points were placed on the mesh surface for monitoring and statistical analysis. A total of seven observation points were arranged laterally and five points longitudinally, as shown in Figures 3 to 6. This setup allows for detailed analysis of the overall acceleration and amplitude fluctuations.

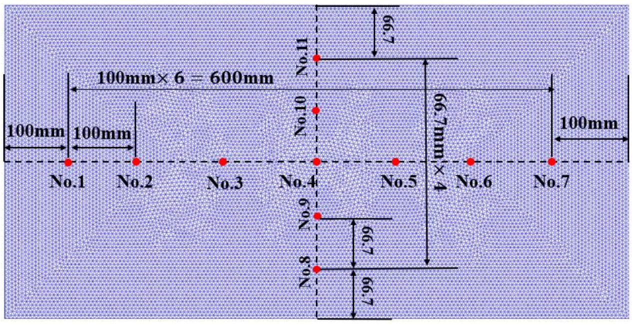

Fig.3 Observation point selection

4. Results and Analysis

4.1. Analysis of Transverse Vibration Characteristics of Mesh Particles

To investigate the vibration characteristics of particles on the mesh surface and obtain accurate variation patterns, seven observation points were selected laterally and five points longitudinally on the mesh surface. The amplitude, acceleration, and stress variations were studied over a frequency range of 10 Hz to 60 Hz.

As shown in Figure 4, from the onset to the end of vibration, the displacement of particles on the mesh surface exhibits periodic variation. Although the magnitudes differ, the overall oscillation patterns are similar. The vibration intensity distribution attenuates and spreads from the excitation source towards both ends. Significant differences in amplitude fluctuations of surface particles are observed at different excitation frequencies. Within the 10 Hz to 20 Hz range, the surface particle fluctuations on the mesh vary slowly with larger oscillation periods and relatively weak vibration amplitudes at all observation points. Over time, wave propagation leads to increased amplitude, and the fluctuation curves of the surface particles exhibit similarity consistent with the standing wave propagation pattern of string vibration, with greater amplitude variation near the excitation source. When the excitation frequency exceeds 20 Hz, observation points 1 to 3, which are farther from the excitation source, display chaotic fluctuations. In contrast, points 4 to 7, closer to the excitation source, exhibit strong periodic oscillations, with pronounced periodic amplitude variations in particles near the excitation source.

Excluding isolated outliers in the data, the average values of the peak amplitude variations for each particle are plotted in Figure 5. When the frequency ranges from 30 Hz to 50 Hz, the amplitude variation interval gradually increases, expanding from approximately -3.49 to 3.98 mm up to -8.06 to 9.62 mm. However, when the frequency exceeds 50 Hz, the amplitude variation range sharply decreases. Analysis indicates that the amplitude fluctuation range progressively enlarges between 30 Hz and 50 Hz, but diminishes beyond 50 Hz, with particles closer to the excitation source exhibiting larger fluctuation intervals.

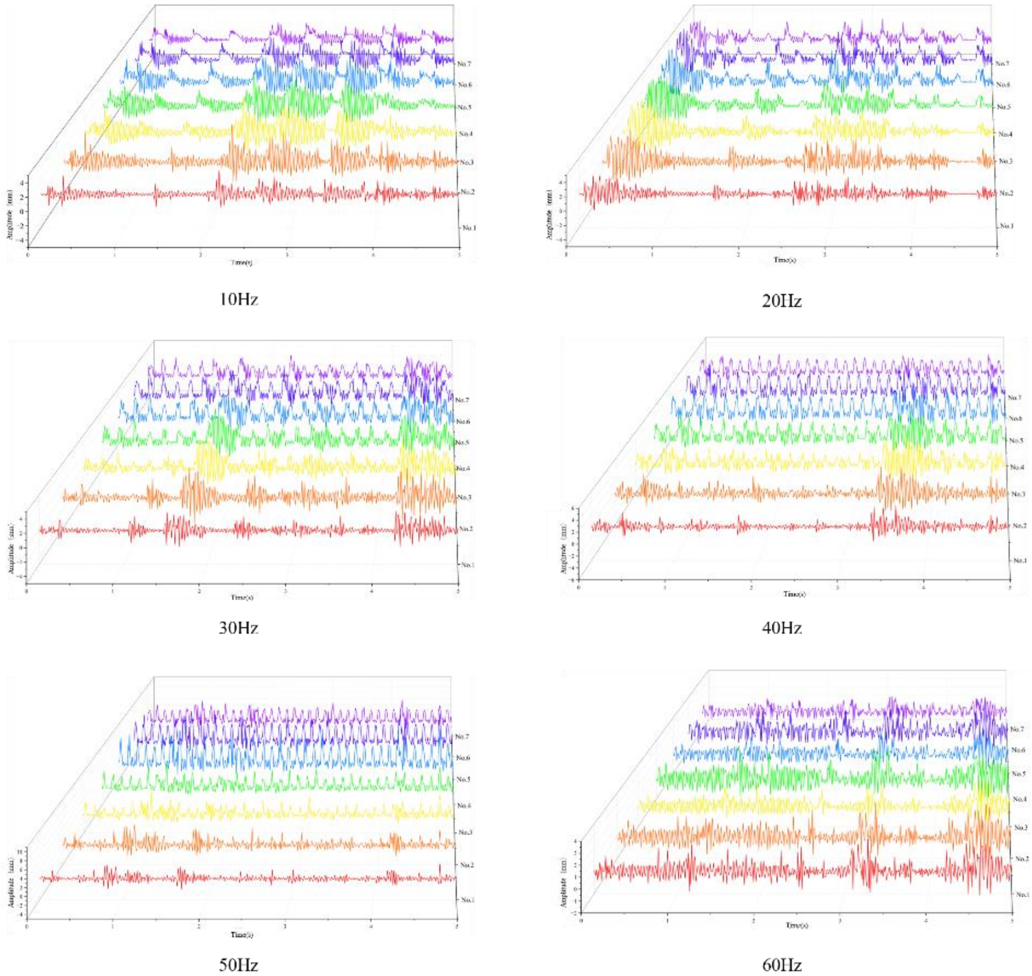

Fig.4 Transverse amplitude variation characteristics of an oscillating mass point

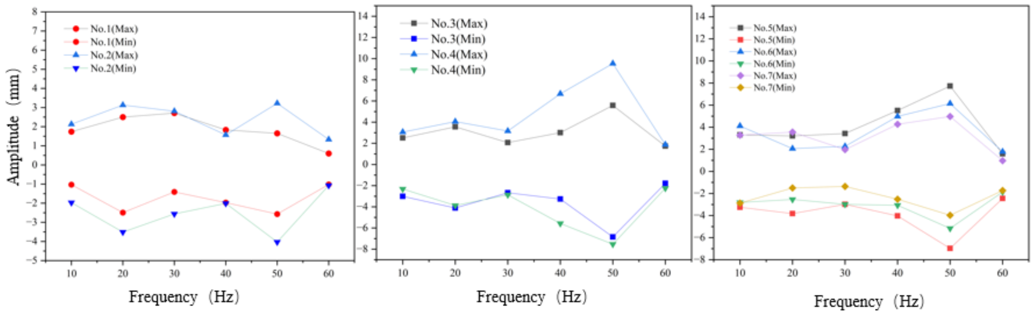

Fig.5 Range of transverse amplitude variation

4.2. Analysis of Longitudinal Vibration Characteristics of Mesh Particles

As shown in Figure 6, from the onset to the end of vibration, the longitudinal vibration of particles on the mesh surface exhibits periodic variation. When the excitation frequency is below 40 Hz, the longitudinal vibration patterns of the particles are generally consistent. However, when the frequency exceeds 40 Hz, significant differences in longitudinal vibration behavior among particles emerge. The figure indicates that low-frequency vibrations do not induce notable longitudinal fluctuations during the string vibration transmission on the mesh. In contrast, at frequencies above 40 Hz, the mesh experiences intense longitudinal oscillations with varying vibration responses among different particles.

Similarly, the mesh demonstrates slow changes and long-period amplitude variations at low frequencies, whereas high-frequency vibrations cause more intense fluctuations longitudinally. Combined with the transverse vibration observations, it is evident that the excitation-induced string vibration of the mesh surface particles propagates not simply as a two-dimensional wave along the x and y axes, but as a complex three-dimensional oscillation resembling the spatial rippling effect created by a stone dropping into water.

This phenomenon helps explain why, when adhesive materials accumulate and block the mesh, vibration frequencies above 40 Hz trigger intense spatial vibrations of the mesh particles. Such vibrations facilitate the point-to-point detachment of filter cakes adhered to the mesh, thereby maintaining the integrity and longevity of the separation membrane and enhancing the efficiency of material dehydration.

Excluding isolated outlier spikes in the data, the average positive and negative amplitude variations of longitudinal particles are plotted in Figure 7. Similar to the transverse amplitude variations, the mesh exhibits a small amplitude variation range at low frequencies. The amplitude variation range increases between 40 Hz and 50 Hz, then decreases when the frequency exceeds 50 Hz. Additionally, the figure shows that the amplitude fluctuation range at both edges of the mesh is larger than that at the center.

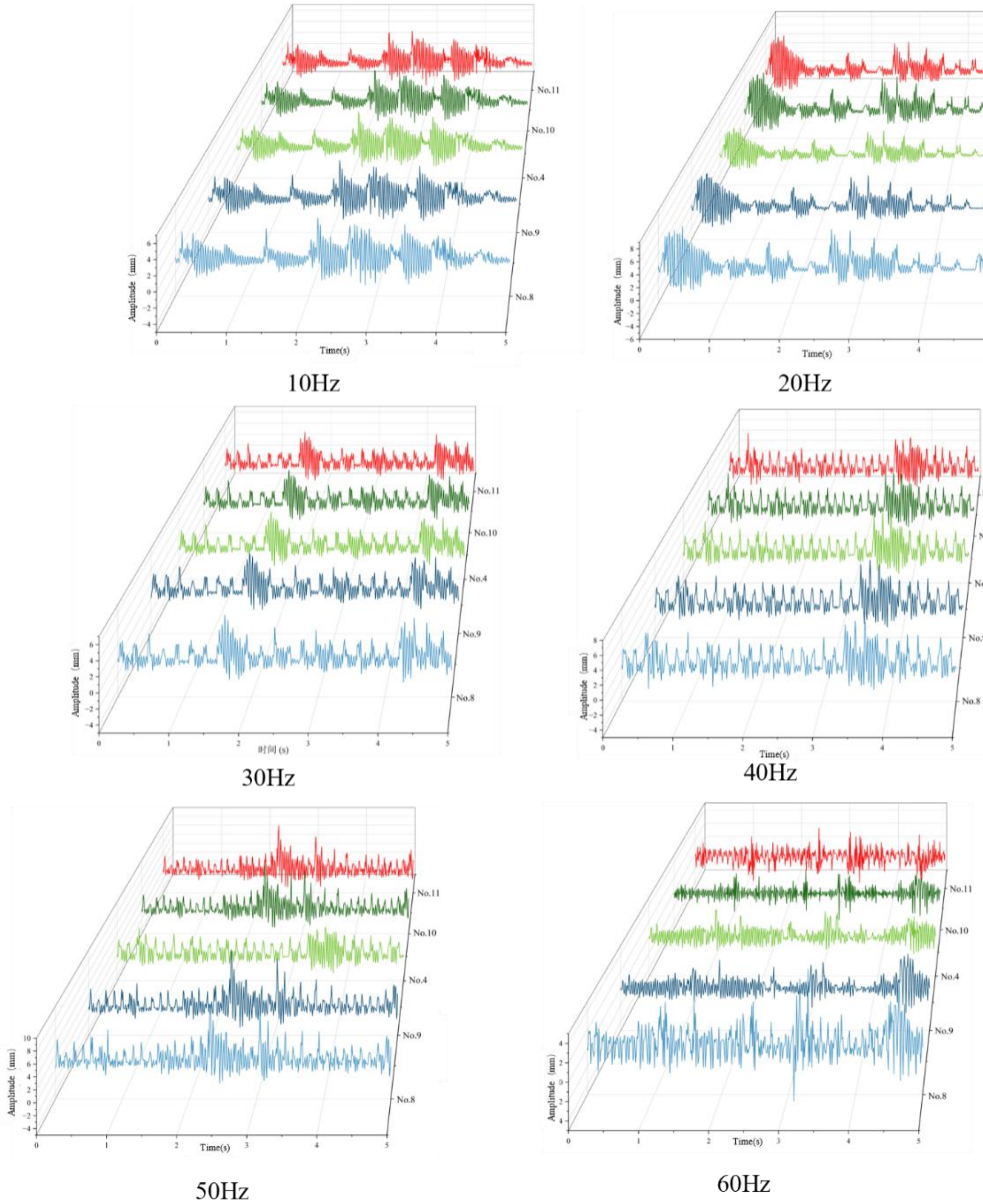

Fig.6 Longitudinal amplitude variation characteristics of an oscillating mass point

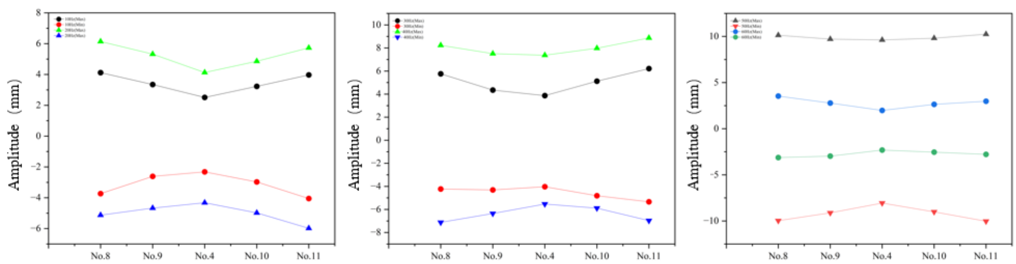

Fig.7 Range of longitudinal amplitude variation

4.3. Analysis of Acceleration Characteristics

The acceleration variation of particles on the mesh surface is illustrated in Figure 8. The acceleration of the mesh particles exhibits periodic fluctuations over time under different excitation frequencies, with notable differences in fluctuation patterns and varying curve trends. The temporal variation of acceleration corroborates the velocity change patterns, showing overall similar curve trends. At 10 Hz, the acceleration variation range is the smallest, fluctuating between 0 and 20 m/s². When the frequency increases to 20 Hz, acceleration ranges from 0 to 80 m/s². With further frequency increases, acceleration grows exponentially; however, the acceleration curves become unstable and display multiple spike-like fluctuations. The particles exhibiting the most intense acceleration fluctuations are located near the excitation source.

At 30 Hz, the acceleration fluctuations show a significant increase compared to lower frequencies, although the overall magnitude remains moderate, and the general curve exhibits consistent motion patterns. At 40 Hz and 50 Hz, pronounced acceleration fluctuations are observed, with intense variations over time and peak acceleration values reaching up to 500 m/s². Across the spatial domain, acceleration ranges mostly remain within ±400 m/s², indicating notable fluctuations. At 50 Hz, the spatial variation trend of acceleration resembles that at 40 Hz, but the differences between positive and negative acceleration fluctuations are more pronounced. Over time, the overall velocity variation trend indicates that 40 Hz is the optimal frequency range. After removing extreme outliers, the average acceleration values of each particle are presented in Figure 9.

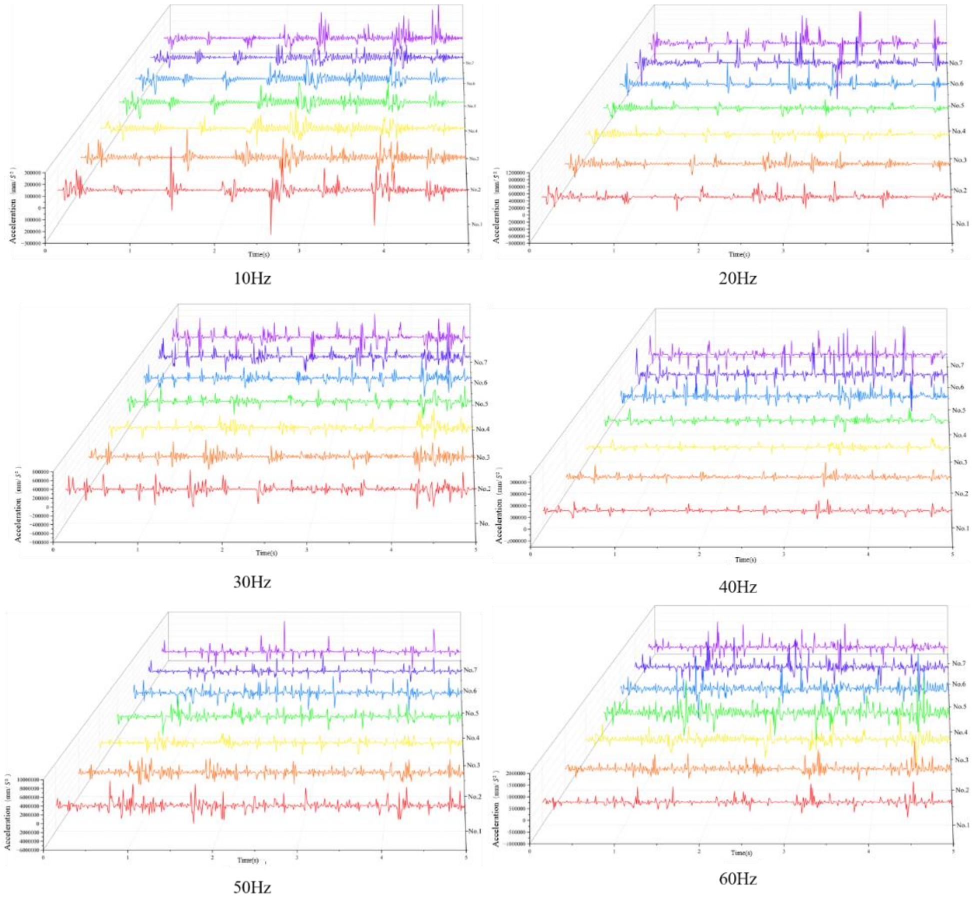

Fig.8 Acceleration variation characteristics

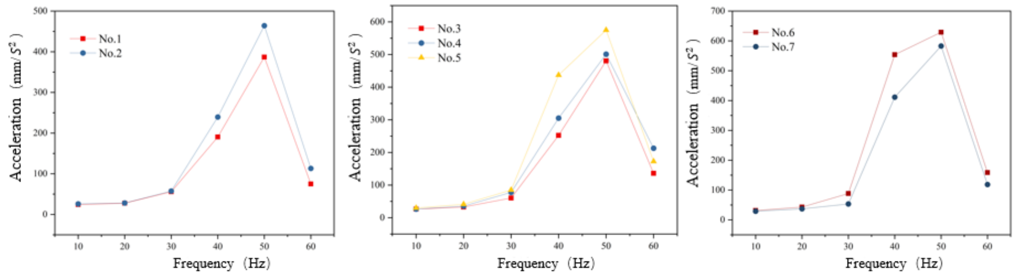

Fig.9 The effect of vibration frequency on the acceleration of each particle

4.4. Analysis of Stress Variation Characteristics on the Filter Screen Surface

When the exciter induces string vibration in the filter screen, the resulting deformation causes variations in shear stress and strain on the filter screen surface. Under these alternating stress conditions, the detachment of filter cake from the screen is facilitated. At a given instant, the stress and strain contour maps of the filter screen surface under different excitation frequencies are shown in Figure 10. The stress and strain contour maps at the same time point under different frequencies are shown in Figure 10. As observed, the variations in stress and strain on the filter screen are not significant when the vibration frequency is below 20 Hz. However, when the frequency exceeds 30 Hz, notable changes in surface stress occur, primarily concentrated near the excitation source. Vertically, the stress on both sides of the filter screen is greater than at the center; this phenomenon disappears between 40–50 Hz, where the stress distribution becomes more uniform, but reappears again above 50 Hz. Horizontally, the surface stress exhibits a segmented distribution pattern. The contour maps illustrate that during string vibration, the oscillations of the filter screen induce the transmission of stress and strain. From maps (c), (d), (e), and (f), it is evident that the maximum stress occurs at the excitation source and gradually diminishes along the length toward both ends.

The stress variation curve of Particle 6, located near the vibration source on the filter screen surface, under different excitation frequencies is shown in Figure 11. As observed, when the frequency is below 20 Hz, the vibration is relatively weak, leading to slow stress variations with long intervals between peak stress values. The peak stress remains below 0.4 MPa, and the overall stress variation trend is relatively consistent. At 30 Hz, although the peak stress remains within 0.4 MPa, the duration of stress fluctuation increases. When the frequency rises to 40–50 Hz, the stress on the filter surface varies significantly, indicating pronounced vibration characteristics in this frequency range. The peak stress increases sharply, reaching approximately 1.5 MPa. However, when the frequency exceeds 60 Hz, the overall stress magnitude rapidly decreases and fluctuates around 0.7 MPa.

In summary, the results demonstrate that excitation frequencies of 40 Hz and 50 Hz induce intense fluctuations in stress and strain on the filter screen surface, which is more favorable for the detachment of solid-phase particles. The variation in the peak stress value on the filter surface with respect to frequency is illustrated in Figure 12.

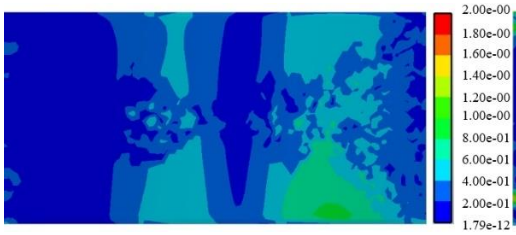

(a) a=10Hz

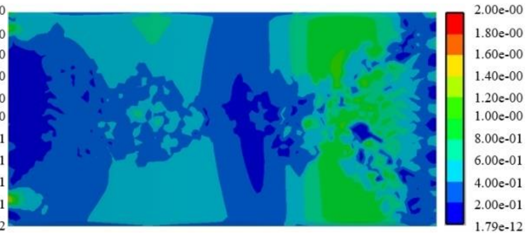

(b) b=20Hz

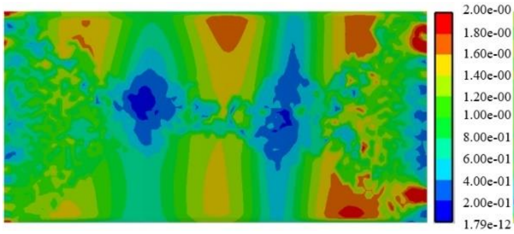

(c) c=30Hz

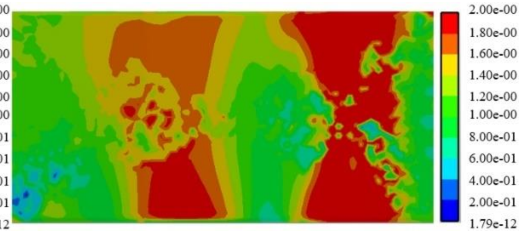

(d) d=40Hz

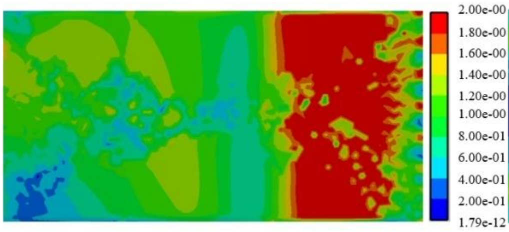

(e) e=50Hz

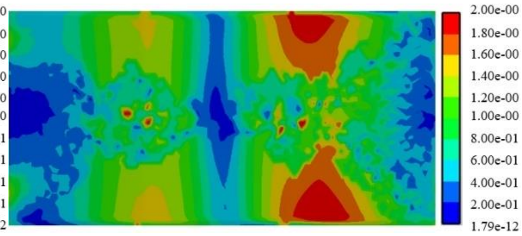

(f) f=60Hz

Fig.10 Stress-strain diagram

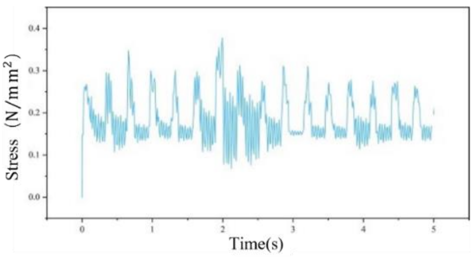

10Hz

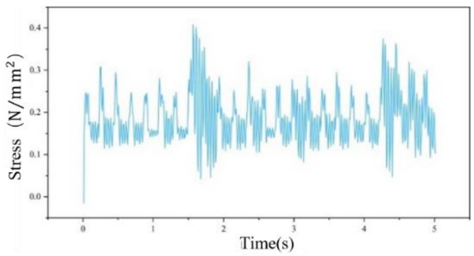

20Hz

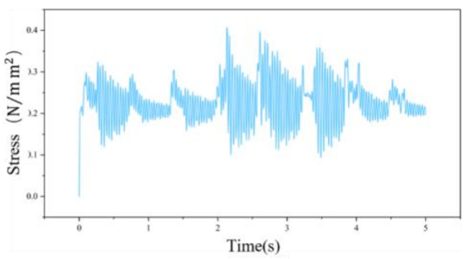

30Hz

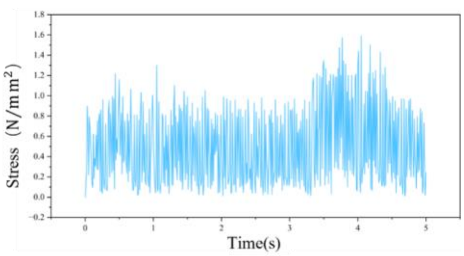

40Hz

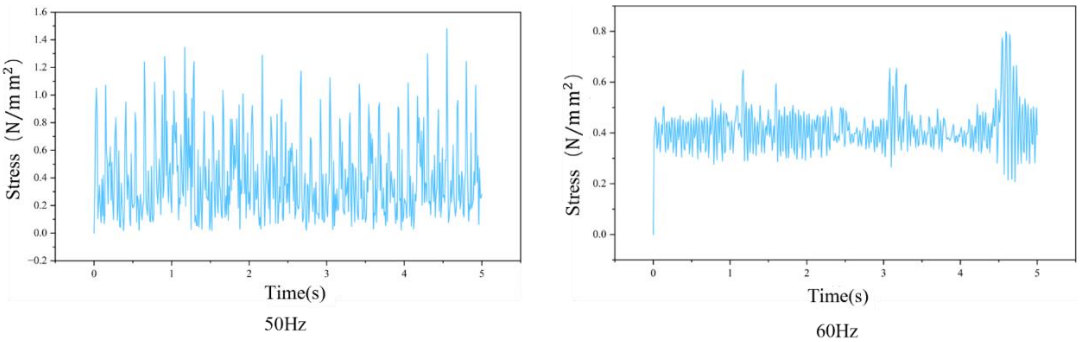

Fig.11 Stress Variation Curve of Surface Particles on Filter Mesh

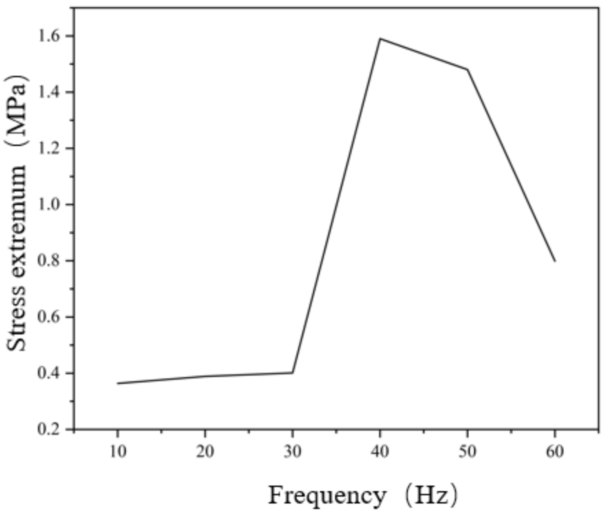

Fig.12 Stress extreme value change curve

5. Conclusion

This study employs a multi-flexible-body dynamics approach to simulate the vibration characteristics of different particles on the filter screen under varying excitation frequencies, as well as the overall stress distribution and the stress variation at the same point on the filter screen at a given time. The results indicate that:

(1) The amplitude fluctuation of particles on the filter screen surface under different excitation frequencies exhibits a parabolic trend with respect to frequency. The fluctuation range of particle amplitude is greater at the edges of the screen than at the center. At 40 Hz, the amplitude fluctuation is most pronounced, and particles near the excitation source display strong periodic oscillations.

(2) The acceleration of filter screen particles varies significantly with frequency, exhibiting intense fluctuations in the 40–50 Hz range. The particle acceleration on the screen surface changes periodically, with particles near the excitation source experiencing rapid velocity fluctuations. When the frequency exceeds 40 Hz, acceleration increases sharply, followed by a rapid decline beyond 60 Hz.

(3) Compared to traditional vibrating screens, the string vibration process induces non-uniform oscillations across different particles on the filter screen surface. The acceleration levels are higher and vary more rapidly than those in conventional systems, making material detachment more efficient.

References

[1] Halabi M A, Al-Qattan A, Al-Otaibi A. Application of solar energy in the oil industry—Current status and future prospects[J]. Renewable and Sustainable Energy Reviews, 2015, 43: 296-314.

[2] Ilyin S O, Strelets L A. Basic fundamentals of petroleum rheology and their application for the investigation of crude oils of different natures[J]. Energy & Fuels, 2018, 32(1): 268-278.

[3] Su, Y. N.; Lu, B. P.;Liu, Y. S.;Zhou, Y. C.;Liu, X. S.;Liu, W.;Zang, Y. B. Pereira L B, Sad C M S, Castro E V R, et al. Environmental impacts related to drilling fluid waste and treatment methods: A critical review[J]. Fuel, 2022, 310: 122301.

[4] Yang J, Sun J, Wang R, et al. Treatment of drilling fluid waste during oil and gas drilling: A review[J]. Environmental science and pollution research, 2023, 30(8): 19662-19682.

[5] Guo C. Current Status and Prospects of Waste Oil-Based Drilling Fluid Treatment Methods in China[C]//International Petroleum and Petrochemical Technology Conference. Singapore: Springer Singapore, 2020: 94-104.

[6] Kang X, Zhang J, Sun F, et al. A review of polymer EOR on offshore heavy oil field in Bohai Bay, China[C]//SPE Asia Pacific Enhanced Oil Recovery Conference. SPE, 2011: SPE-144932-MS.

[7] Santos J M, Pereira M S, Júnior I P, et al. Microwave drying of drilled cuttings in the context of waste disposal and drilling fluid recovery[J]. Energy Technology, 2014, 2(9-10): 832-838.

[8] Grabsch A F, Fawell P D, Davies M G. Flocculating fine cuttings particles suspended within partially hydrolysed polyacrylamide (PHPA) solutions used as drilling fluids in mineral exploration[J]. Minerals Engineering, 2024, 206: 108510.

[9] Chen J,Wu S,Luan J,et al. Development and application of a novel integrated treating equipment for waste drilling fluid[J].Fresenius Environmental Bulletin,2020,29(5):3984-3991.

[10] Song B, Liu C,Peng L,et al. Dynamic analysis of new type elastic screen surface with multi degree of freedom and experimental validation[J]. Journal of Central South University,2015,22(4):1334-1341.

[11] Yin P, Hou Y. Dynamic study on particle throwing motion of pulsating negative pressure shale shaker[J].Journal of Petroleum Exploration and Production Technology,2023,13(2):753-762.

[12] Menezes A L,Barbosa V P,Malagoni R A,et al. Evaluation of the residual moisture content in pilot scale vibrating screening operating with pressure reduction in the screen drying region[J].Powder Technology,2020,369:17-24.

[13] Nuraliyev A, Ibadullayev M . Research and development of resonant electromagnetic vibration screen for intensive vibration technologies[J].E3S Web of Conferences,2020,216:01114.

[14] Gong Jianhui, Wang Chenfeng, Yao Jing, et al. Visualization Study of String Vibration [J]. Inner Mongolia Science & Technology and Economy, 2021(18):109-110, 127.

[15] Zhang Xinggang, Kong Weishu. Theoretical Study and Numerical Simulation of Elastic String with Both Ends Fixed [J]. Journal of Shandong University (Science), 2008(10):71-76.